

High count rate γ -ray spectroscopy with $\text{LaBr}_3\text{:Ce}$ scintillation detectors

B. Löhner^{*,a,b}, D. Savran^{a,b,c}, E. Fiori^{a,b}, M. Miklavc^c, N. Pietralla^d, M. Vencelj^c

^a*ExtreMe Matter Institute EMMI and Research Division, GSI Helmholtzzentrum für Schwerionenforschung, Planckstr. 1, 64291 Darmstadt, Germany*

^b*Frankfurt Institute for Advanced Studies FIAS, Ruth-Moufang-Str. 1, 60438 Frankfurt am Main, Germany*

^c*Innovation Centre for Advanced Sensors and Sensor Systems, INCAS³, Assen, The Netherlands*

^d*Jožef Stefan Institute, Jamova cesta 39, 1000 Ljubljana, Slovenia*

^e*Institut für Kernphysik, TU Darmstadt, Schlossgartenstr. 9, 64289 Darmstadt, Germany*

Abstract

The applicability of $\text{LaBr}_3\text{:Ce}$ detectors for high count rate γ -ray spectroscopy is investigated. A 3"×3" $\text{LaBr}_3\text{:Ce}$ detector is used in a test setup with radioactive sources to study the dependence of energy resolution and photo peak efficiency on the overall count rate in the detector. Digitized traces were recorded using a 500 MHz FADC and analysed with digital signal processing methods. In addition to standard techniques a pile-up correction method is applied to the data in order to further improve the high-rate capabilities and to reduce the losses in efficiency due to signal pile-up. It is shown, that γ -ray spectroscopy can be performed with high resolution at count rates even above 1 MHz and that the performance can be enhanced in the region between 500 kHz and 10 MHz by using pile-up correction techniques.

Key words: digital pulse shape analysis, γ -ray spectroscopy, lanthanum bromide, scintillator

1. Introduction

In modern nuclear physics experiments γ -ray spectroscopy is one of the major tools to investigate the structure of stable and unstable nuclei. The detection and spectroscopy of the emitted photons in the de-excitation of particle-bound excited states is a mandatory ingredient in many studies of nuclear reactions. Consequently γ -ray detectors play an important role in the configuration of experimental setups.

Different types of detectors are available. The optimum choice depends on the requirements of the γ -ray spectroscopy experiments. High-Purity Germanium (HPGe) detectors are often used for highest resolution, while several scintillator based detectors provide better timing properties (at the cost of reduced energy resolution) or are more suited for high acceptance spectrometers due to their much lower costs.

In many experiments, the emitted γ rays in the reaction of interest are accompanied by a rather large γ -ray

background close to the target position. This radiation originates from photons produced in background reactions such as bremsstrahlung by fast secondary electrons or reactions within the beam dump or other material along the beamline. Since it is difficult (or even unwanted) to suppress this intense background one often has to deal with high count rates. To avoid signal distortion, the maximum count rate capability of each detector must not be exceeded. As a consequence the rate in the photon detectors often limits the beam intensity and therefore the reaction rate.

The recently developed scintillator material lanthanum bromide ($\text{LaBr}_3\text{:Ce}$, tradename $\text{BrilLanCe}^{\text{TM}}$ 380 by Saint Gobain [1]) is well suited to push the limitations posed by this problem. Its excellent timing properties (down to 100 ps in optimal conditions [2–4]), temperature stability [5, 6] and high energy resolution for a scintillator (3% at 662 keV [7, 8]), which is dominated by statistical contributions [9], have made $\text{LaBr}_3\text{:Ce}$ the material of choice for many nuclear physics experiments including γ -ray spectroscopy [10, 11], medical imaging [12, 13] or industrial applications [14, 15]. The high light yield (165% of that of NaI) and the very short scintillation light decay constant (between 20 and 30 ns [5, 6])

*Corresponding address: ExtreMe Matter Institute EMMI and Research Division, GSI Helmholtzzentrum für Schwerionenforschung, Planckstr. 1, 64291 Darmstadt, Germany, Tel.: +49 6159711803; fax: +49 6159713475

Email address: b.loeher@gsi.de (B. Löhner)

Preprint submitted to Elsevier

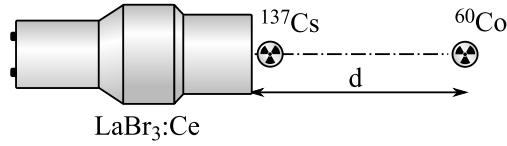


Figure 1: A schematic illustration of the experimental setup. The weaker ^{137}Cs source was kept at a fixed distance to the detector (close to the front cap to get the highest count rate possible), while the distance of the strong ^{60}Co was varied to create a variable amount of background radiation.

pose $\text{LaBr}_3:\text{Ce}$ as a well suited candidate material to allow γ -ray spectroscopy at very high count rates. This property has been briefly discussed by comparing $\text{LaBr}_3:\text{Ce}$ to NaI [2]. However, the investigation in [2] does not include the study of efficiency and resolution – the key properties for nuclear physics experiments – when increasing the count rate in the $\text{LaBr}_3:\text{Ce}$ detector.

In this article we investigate in greater detail the high count rate capabilities of $\text{LaBr}_3:\text{Ce}$. The energy resolution as well as the photo peak efficiency are studied with respect to the count rate. For further improvement it is possible to introduce digital signal-processing (DSP) techniques to correct signal distortions and restore efficiency losses due to pile-up. It is shown that high-resolution γ -ray spectroscopy with $\text{LaBr}_3:\text{Ce}$ detectors is possible at count rates well in excess of 1 MHz. Simulations with synthetic signals have been carried out to investigate the limits of this approach, and to support the experimental results.

Section 2 of this article will shortly introduce the experimental setup that was used for the measurements, while the data analysis, including feature extraction from the digitized signals, are detailed in Section 3. This section also describes how a timestamp-based pile-up correction method, first introduced in [16], can be used to further improve the performance of $\text{LaBr}_3:\text{Ce}$ detectors at high count rates. In Section 4 the results of these investigations will be shown. An outlook for future investigations is presented in Section 5.

2. Detector and Setup

The experimental setup for the present investigation is shown in Fig. 1. The large volume 3”x3” $\text{LaBr}_3:\text{Ce}$ detector was irradiated by two different radioactive sources. One ^{137}Cs source of medium activity (45 kBq) was placed in contact with the front face of the detector, while a ^{60}Co source with high activity (73 MBq) was placed at a variable distance d . The ^{137}Cs source was fixed in place for all measurements and thus provides

the stable reference, while the strong ^{60}Co source was moved within a range of 5-100 cm in order to vary the overall count rate. The count rate using only the ^{137}Cs source was 10 kHz. Bias voltage for the Hamamatsu R10233 photomultiplier tube (PMT) was delivered from an *iseq* NHQ-203M power supply through a 2007 voltage divider base from Canberra and operated at bias voltages from 300 V to a maximum of 1200 V. The anode signal of the PMT was amplified by a fast timing filter amplifier (TFA) with 1 μs differentiation and 1 ns integration time settings in order to match the dynamic range of the sampling ADC. The amplified signal was then recorded with a Struck SIS3350 digital sampling ADC with a sampling rate of 500 MHz and a resolution of 12 bit [17]. The length of each signal trace was set to 10^5 data points corresponding to 0.2 ms of continuous samples. To reach a live time of 2 s, in total 10^4 traces have been recorded for each distance d . Data acquisition was done using a Struck SIS3104/SIS1100e PCIe-VME-interface and a standard PC running the GECKO data acquisition software[18] with online signal processing. Using the PCIe-VME-interface high data transfer rates of more than 100 MB/s between the VME electronics and the PC could be reached to allow fast readout of the sampling ADC.

3. Signal analysis and pile-up correction

The information conveyed in the digitized signals first has to be extracted using DSP methods that are described in this section. At first the timestamp is extracted from the fast rising edge of the pulse, because the steepest part of the slope conveys precise timing information. Afterwards regions of the trace without any signals are identified based on the timestamps. Then the baseline offset is corrected. The energy deposit information can then be extracted from the integral over each signal. These parts of the data analysis are described in detail in the following.

3.1. Feature extraction

Several different steps of signal analysis are performed on the data in order to extract the basic signal information (i.e. energy and timing). The baseline-offset voltage is estimated by averaging over 10 data points of the signal trace in regions where no γ -ray signal is present and is then subtracted from the original signal. At very high count rates the probability for such “empty” regions in a trace decreases, such that the determination of the baseline becomes more difficult. At the cost of precision it is still possible to derive a value

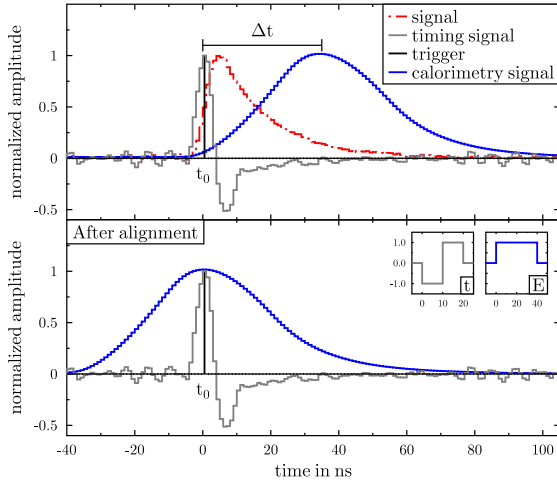


Figure 2: *Top*: A differentiating filter (t) transforms the signal (dashed, red line) into the timing signal (grey). After filtering with an integrating box filter (E), the signal is transformed into a calorimetry signal (solid, blue). The delay Δt between these two signals is independent of the amplitude. The trigger time t_0 is determined from the timing signal. *Bottom*: After taking into account the delay Δt , the amplitude of the signal is determined at the time t_0 .

for the baseline, if the trace contains at least one of such regions. If no suitable regions are present, then different methods have to be employed, which however was not necessary in the present case. The dashed red line in Fig. 2 shows a typical signal trace with the baseline offset voltage already subtracted. To derive a reference point in time (trigger time or timestamp) from this signal, the data are convoluted with a discrete bipolar Finite Impulse Response (FIR) filter kernel with a width that equals the signal rise time. It is possible to assume an energy independent rise time of about 10 ns, because the signal shape does not depend on the energy. This filter kernel has the value -1 for the first 10 ns and the value $+1$ for another period of 10 ns (see inset "t" in the lower panel of Fig. 2). The resulting bipolar timing signal is shown in gray. From the maximum of this timing signal it is possible to derive an accurate trigger timestamp, which is denoted as t_0 in the illustration.

In the next step the deposited energy is determined by integrating the signal. The original signal is filtered with a unipolar FIR filter kernel, i.e. its value is $+1$ over its duration, with a width that ideally equals the length of the signal (shown with a width of 40 ns in inset "E"), in order to produce an integrated calorimetry signal (solid blue). For computational reasons the width of the filter can be reduced at the cost of precision. In the present analysis a width of 40 ns was used for all of the measurements. The amplitude of this calorimetry sig-

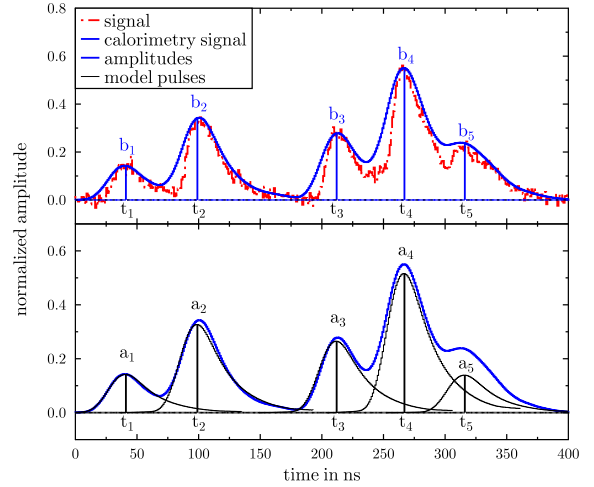


Figure 3: *Top*: Example of a pile-up situation. Amplitudes (blue) have been measured from the calorimetry filtered signal (solid line). *Bottom*: After pile-up correction the measured amplitudes b_i are corrected to yield the true amplitudes a_i (black). The superposition of the model pulse shapes (thin lines) results in the filtered signal (thick line).

nal corresponds to the amount of deposited energy. The resulting timing and calorimetric signals are aligned in time by shifting them with respect to each other, as denoted in Fig. 2 by Δt . The value of this delay is constant for any recorded signal, as long as the signal shape is constant, which is the case in the present study. The energy deposit is thus given by the value of the calorimetry signal at $t = t_0 + \Delta t$. This approach for extracting the signal properties has been chosen for two reasons: First this is an exceedingly simple and numerically stable approach, and more importantly this approach allows for a correction of the measured amplitudes in the case of strong pile-up, as described in the following.

3.2. Pile-Up correction

At increasing count rates the average time difference between two consecutive pulses will be shorter than the individual pulse length. Consequently different pulses overlap in time, resulting in a correlation of their properties, which – if not corrected for – finally leads to a reduction of the energy resolution and a loss of photopeak efficiency. The pile-up correction method that was used in the analysis has first been presented in [16]. The detailed description can be found there, and only a short outline is given in this article.

This method relies on the assumption that the pulse shape of every signal from the same scintillation detector is stable and independent from its amplitude, so that the complete signal trace can be expressed as a linear

combination of single pulses, as illustrated in Fig. 3. This assumption is sufficiently well fulfilled. The complete trace can thus be described by the timestamp of each pulse and the corresponding pulse amplitude, as well as a single model pulse shape common to all pulses that characterizes the dynamics of a single signal. Based on this model the correlation of neighboring signals can be resolved in order to restore the correct γ -ray energy information from the measured amplitudes.

Figure 3 illustrates the principle of the applied pile-up correction method. A signal trace (dashed red) with five signals from the LaBr₃:Ce detector is shown at the top together with the computed calorimetry signal (blue solid). For illustration purposes the time delay introduced by the digital filters is removed as described above. The single signals partly overlap each other, such that the amplitudes b_i taken from the calorimetry signal at times t_i signal are overestimated (especially visible in the case of b_4 and b_5). The solution to correct for this overestimation is to treat each of the amplitudes b_i as a superposition of the true amplitude a_i of the corresponding signal and additional contributions c_i from the surrounding signals:

$$b_i = a_i + \sum_{\substack{j=0 \\ j \neq i}}^N c_j. \quad (1)$$

The contribution of the j th neighbor signal can be expressed as the true amplitude a_j of the neighbor signal weighted with a factor m_{ij} , such that $c_j = m_{ij}a_j$. The value of this factor depends solely on the time difference $t_{ij} = t_i - t_j$ between the time of signal i and the time of the neighbor j and can be derived with the use of the model pulse shape $m(t)$. Taking the value of the model pulse shape at the time t_{ij} with respect to the trigger time t_0 of the model pulse yields the desired weight $m_{ij} = m(t_0 + t_{ij})$, resulting in

$$b_i = \sum_{j=0}^N m_{ij}a_j = \sum_{j=0}^N m(t_0 + t_{ij})a_j. \quad (2)$$

For all signals in the trace this equation can be written as a set of linear equations

$$\mathbf{b} = \mathbf{M}\mathbf{a}, \quad (3)$$

that can be solved by inverting the matrix \mathbf{M} containing the weights m_{ij} and thus produce a solution for the true amplitudes a_i

$$\mathbf{a} = \mathbf{M}^{-1}\mathbf{b}. \quad (4)$$

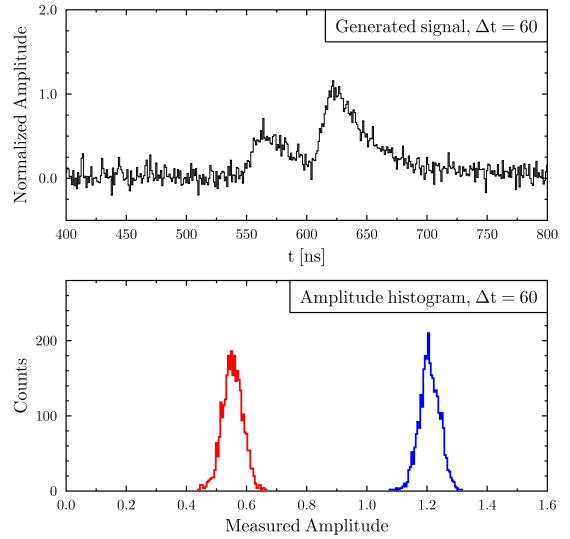


Figure 4: *Top*: Generated signal group with a distance of $\Delta t = 60$ ns between the two signals. *Bottom*: Amplitude histograms determined for many generated sets of two pulses at $\Delta t = 60$ ns. Distribution of first pulse amplitude shown in red (at 0.5), second pulse amplitude in blue (at 1.15).

The model pulse shape is determined using data recorded with a low count rate, in order to avoid pile-up situations. From this data a large number of single signals are extracted. These signals are averaged and normalized to amplitude 1.0 to produce the model pulse shape.

The bottom part of Fig. 3 shows the same calorimetry signal again, but now together with the computed amplitudes a_i and the corresponding constituent signals (black). These constituent signals are produced by scaling the model pulse shape with the true amplitude a_i as determined using Eq. 4 and shifting it in time to match the trigger time t_i . From this figure it is obvious, that the calorimetry signal results from a superposition of all constituent signals. The free parameters of this algorithm are the extents of the matrix \mathbf{M} , which control how many neighbor signals to take into account for each calculation. It is reasonable to assume a small number of rows and columns, because the model pulse shape only has non-zero elements within about 200 ns around its trigger time. This fact allows to calculate the matrix inversion with only a small amount of computing resources, and even enables the implementation of the algorithm in hardware for real-time applications (e.g. FPGA or DSP as in [19]).

3.3. Application limits

To study the performance of the digital signal analysis and the limits for the application of the pile-up cor-

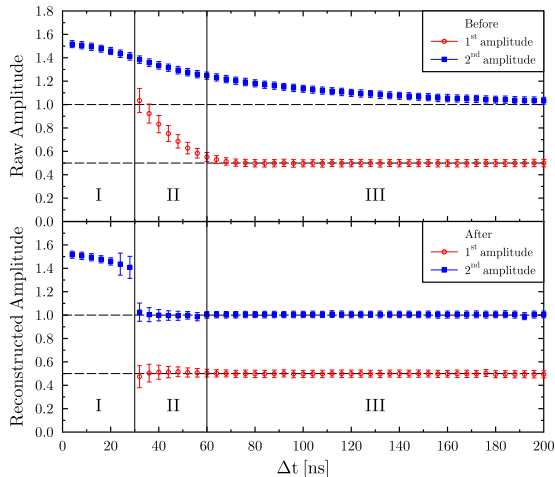


Figure 5: *Top*: Measured raw amplitudes (b_i) with respect to time difference Δt (first signal with squares, second with circles). Horizontal lines indicate "true" generating amplitudes. Uncertainties in each point result from statistical errors. Three distinct ranges in Δt can be identified: (I) Signals are indistinguishable (II) Incorrect amplitudes due to pile-up (III) First amplitude is measured correctly, but second one is still overestimated. *Bottom*: Reconstructed amplitudes (a_i). Three distinct regions can be identified: (I) Trigger limited mis-identification, (II) Transition region with increased uncertainty on the result, (III) Incorrectly measured amplitudes are accurately restored.

rection algorithm, test cases have been constructed with two synthetic signals at a well defined distance Δt . The upper part of Fig. 4 shows an example with a distance of $\Delta t = 60$ ns and an amplitude ratio of 1:2 of the two signals (the second is twice as large as the first). The signals are generated from an exponential function with a decay constant of 60 ns, which is smoothed with a gaussian filter to create a finite rise time of about 20 ns (matching the properties of real detector signals) and then scaled to its amplitude. White Gaussian noise is added to the trace to produce a signal-to-noise ratio (SNR) of 10 for the first and 20 for the second signal, respectively (SNR is here defined as pulse height divided by the root mean square of the noise level). This amount of noise is chosen to simulate small detector signals. For these small signals the limitations of the method with respect to timing are more visible when compared to large signals. The parameter Δt is varied from 0 to 200 ns in steps of 4 ns, and for each step a set of 5000 traces was generated. Due to the random noise all generated traces in each set differ from each other. The traces were analysed with the same approach described in Sec. 3.1 to determine the trigger times t_i and the raw amplitudes b_i of the two signals. For each Δt a histogram (lower part of Fig. 4) was filled with the determined amplitudes, and

a gaussian distribution was fitted to determine the mean value and the FWHM of each of the two peaks.

The results are shown in the upper part of Fig. 5 as a function of the time difference Δt of the two generated signals. The error bars for each point are drawn according to the determined FWHM. Three distinct ranges in Δt can be identified: (I) The time difference is comparable to or even smaller than the rise time of the signals. They appear as one single signal and the trigger algorithm cannot distinguish between them; (II) At intermediate time distances, both amplitudes are incorrectly measured, because of pile-up. This region extends to about three times the rise time for our simulation; (III) The first amplitude is measured correctly, because in this region the influence of the rising edge of the second signal on the amplitude of the first one becomes negligible. The amplitude of the second signal is still overestimated (top of Fig. 5).

The lower part of Fig. 5 shows the results after the pile-up correction method has been applied. For this simulation the method only takes into account the next neighbors of each signal (1st order), because only two signals participate. The three different regions can be identified here as well: Region (I) is the region of unresolvable pile-up, where the pile-up correction cannot be applied, because the two signals cannot be separated. For the same reason it is not possible to reject these signals, based purely on the trigger information. Region (II) is the transition region, where the pile-up correction method can be applied, and yields the proper result. However, for shorter time intervals the statistical uncertainty increases. Depending on the application, the events in this transition region can be identified and rejected. Besides depending on the detector resolution, these signals may be corrected well enough to contribute to the photo peak. The amplitudes in region (III) can be properly restored within their intrinsic uncertainties.

The simulation shows that in a range of 60-200 ns for Δt the pile-up correction method yields a good reconstruction of the signal amplitude, while the uncorrected amplitude of the second signal is determined incorrectly. When applying the same method to real data an improvement of the extracted properties is expected for count rates where a large fraction of the signals have a distance in this range. At lower or higher count rates the improvement is expected to be much smaller, because either an insignificant amount of signals overlap or because the average distance between two signals is too small to allow for precise determination of the time-stamp.

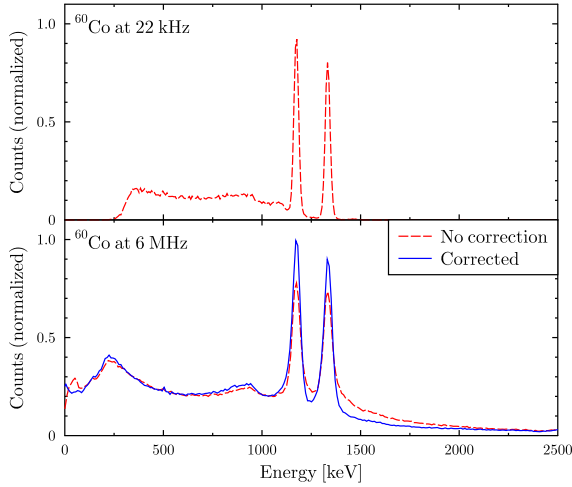


Figure 6: (Color online) Energy spectra of emitted γ -rays from a ^{60}Co source recorded with the $\text{LaBr}_3\text{:Ce}$ detector. *Top*: Large distance (1.5 m) between source and detector to induce a low count rate of 22 kHz. *Bottom*: The count rate increases to 6 MHz at smaller distances (20 cm). Pile-up events are visible above energies of 1.3 MeV in the spectrum without correction (dashed red). These are partly restored in the corrected spectrum (solid blue).

4. Experimental results

In this section the experimental results from the measurements detailed in Sec. 2 are presented.

Figure 6 shows energy spectra of emitted γ -rays from the strong ^{60}Co source recorded with the $\text{LaBr}_3\text{:Ce}$ detector. For this data only the ^{60}Co source has been used. The top part shows the spectrum taken with a low count rate, while the source was placed at a distance of 1.5 m to the detector. The lower part of Fig. 6 shows the spectrum when recorded with the source at a distance of 20 cm. The count rate increases from 20 kHz to 6 MHz and pile-up events become apparent in this spectrum, which can be seen as high energy tails of the peaks and the increase of events with energies much larger than 1.33 MeV. Without pile-up correction the red (dashed) spectrum has less photo peak efficiency (5% peak-to-total compared to 16% at 20 kHz) and also the energy resolution is worse when compared to the spectrum at low count rates (see Fig. 7). After pile-up correction taking into account up to three neighboring signals on each side (blue) the photo peak efficiency (8% peak-to-total) as well as the energy resolution are partly recovered. At the same time the number of pile-up events above 1.33 MeV is reduced to 62%.

The photo peak efficiency is determined from the peak area of the 661 keV peak corresponding to the energy of the γ -rays emitted by the ^{137}Cs source. The peak

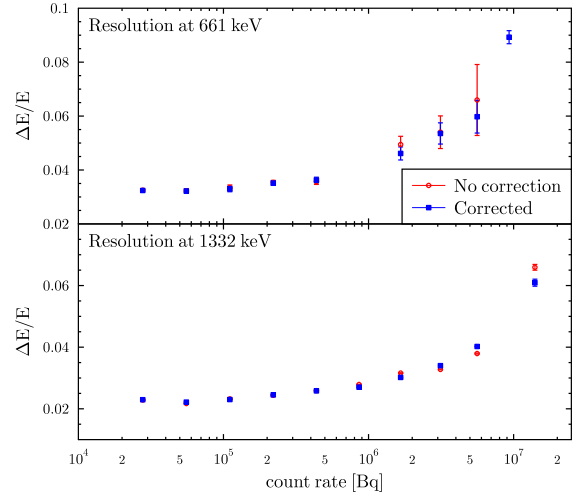


Figure 7: *Top*: Relative resolution at 661 keV (^{137}Cs) without correction (red circles) and with correction (blue squares). At the highest count rate the resolution without correction could not be determined. *Bottom*: Relative resolution at 1332 keV (^{60}Co).

region has been fixed for all count rate settings. The obtained values are then normalized to the peak area at the lowest count rate of 28 kHz.

The dependence of the energy resolution and photo peak efficiency on the count rate has been studied quantitatively. The results are presented in Figs. 7 and 8 respectively. The energy resolution stays below 4% at 661 keV for count rates below 500 kHz, and does not increase above 10% for the highest count rate measured (14 MHz). The same is true for the resolution at 1332 keV. From Fig. 7 it is also clear that the pile-up correction (blue squares) restores the energy resolution, but not by a significant amount. The lengths of the error bars correspond to statistical errors only. For the highest count rate the uncorrected spectrum could not be analysed.

In the upper part of Fig. 8 the results for the relative photo peak efficiency at 661 keV is shown. Again red circles indicate the efficiency before pile-up correction, and blue squares mark the results after pile-up correction. Along with the data points two different curves are drawn. These curves correspond to the probability that within a certain time interval τ a second following signal occurs, if a random sequence of signals is assumed. These probabilities are calculated using a Poisson distribution, according to

$$P(N, n) = \frac{(n\tau)^N e^{-n\tau}}{N!}, \quad (5)$$

where N denotes the number of signals in the time in-

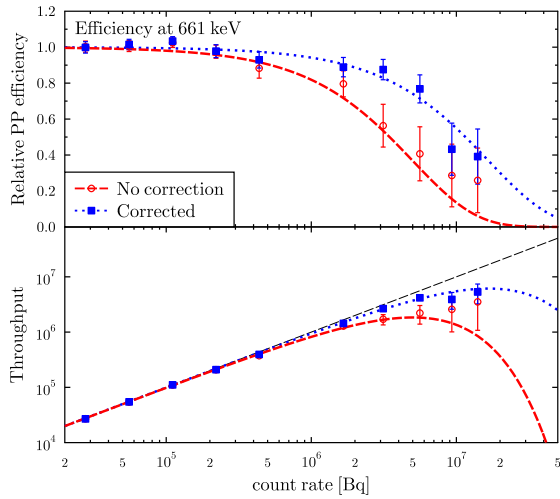


Figure 8: *Top*: Relative photo peak efficiency at 661 keV normalized to the value at the lowest count rate (red circles without correction, blue squares with correction). The curves indicate the probability for detecting only one signal within a time interval τ (dotted: $\tau = 60$ ns, dashed: $\tau = 200$ ns) at the respective count rate. *Bottom*: Throughput (product of relative PP efficiency and count rate). At count rates above 1 MHz a clear enhancement is visible after correction. The curves are calculated from the above probability characteristic.

terval of length τ and n the mean number of pulses per time interval (count rate). Thus, $P(0, n)$ is the probability for a second pulse occurring within the time τ for a given count rate n . For the illustration two different values for τ (blue: $\tau = 60$ ns, red: $\tau = 200$ ns) as estimated from the simulation in Sec. 3.3 are used. The measured data follow the shape of the two curves in both cases, which indicates that the simulation correctly predicts the region where the application of the pile-up correction method will improve the results. In the range between 500 kHz and 10 MHz the advantage from using the pile-up correction method is most noticeable. For lower count rates the effect of pile-up can be neglected, while for higher count rates the leading edges of the pulses overlap and thus prohibit accurate triggering. The lower part of Fig. 8 shows the resulting estimated throughput (given by the product of relative efficiency and the count rate) together with the ideal case where the throughput equals the incoming count rate (black line) and the two curves from the theoretical prediction. This figure demonstrates, that at a low count rate the effect of pile-up correction is negligible, while at count rates above 1 MHz the improvement is significant, increasing the ideal count rate and the maximum throughput by a factor of 3.

5. Conclusions and Outlook

The analysis has shown that LaBr₃:Ce detectors are suitable for γ -ray spectroscopy even at very high count rates, exceeding 1 MHz. Using the presented pile-up correction method, the loss of photo peak efficiency from piled-up pulses can be alleviated. A reasonable range for the application of this method is between 500 kHz and 10 MHz, corresponding to an average distance of two signals in the range from 60 to 200 ns. At count rates above 10 MHz the analysis of the digitized signals becomes more demanding, because additional effects decrease the accuracy of feature extraction. One of these effects is the saturation of the PMT with increasing count rate, which can be avoided either with a lower bias voltage or by using an active voltage divider with transistor stages. Other effects that arise at these high count rates like unresolvable pile-up and the fact that the baseline offset can not be determined in a simple manner need additional investigation.

Acknowledgments

The authors thank H. Wörtche (INCAS³), and M. Kirsch (Struck Innovative Systeme) for valuable and inspiring discussions. B.L. and D.S. thank the Institut Jožef Stefan, Ljubljana for their kind hospitality. This work was supported by the Alliance Programme of the Helmholtz Association (HA216/EMMI), by the LOEWE programme of the state of Hesse through the Helmholtz International Center for FAIR, by the Deutsche Forschungsgemeinschaft (SFB 634) and the Innovation Centre for Advanced Sensors and Sensor Systems, INCAS³, Assen, The Netherlands. Further support was provided by the Slovene Competence Center for Biomedical Engineering, and by Instrumentation Technologies of Solkan, Slovenia.

References

- [1] Saint-Gobain Crystals, France, Data sheet of material Bril-LanCe 380 (2008).
- [2] A. Iltis, M. Mayhugh, P. Menge, C. Rozsa, O. Selles, and V. Solovyev, Nuclear Instruments and Methods in Physics Research Section A: Accelerators, Spectrometers, Detectors and Associated Equipment **563**, 359 (2006), ISSN 0168-9002, tRDs for the Third Millennium - Proceedings of the 3rd Workshop on Advanced Transition Radiation Detectors for Accelerators and Space Applications.
- [3] M. Moszynski, M. Gierlik, M. Kapusta, A. Nassalski, T. Szczesniak, C. Fontaine, and P. Lavoute, Nuclear Instruments and Methods in Physics Research Section A: Accelerators, Spectrometers, Detectors and Associated Equipment **567**, 31 (2006), ISSN 0168-9002.

- [4] S. Zhu, F. Kondev, M. Carpenter, I. Ahmad, C. Chiara, J. Greene, G. Gurdal, R. Janssens, S. Lalkovski, T. Lauritsen, et al., Nuclear Instruments and Methods in Physics Research Section A: Accelerators, Spectrometers, Detectors and Associated Equipment **652**, 231 (2011), ISSN 01689002.
- [5] E. V. D. van Loef, P. Dorenbos, C. W. E. van Eijk, K. W. Krämer, and H. U. Güdel, Nuclear Instruments and Methods in Physics Research Section A: Accelerators, Spectrometers, Detectors and Associated Equipment **486**, 254 (2002), ISSN 0168-9002.
- [6] M. Moszynski, A. Nassalski, A. Syntfeld-Kazuch, T. Szczesniak, W. Czarnacki, D. Wolski, G. Pausch, and J. Stein, Nuclear Instruments and Methods in Physics Research Section A: Accelerators, Spectrometers, Detectors and Associated Equipment **568**, 739 (2006), ISSN 0168-9002.
- [7] F. Quarati, A. Bos, S. Brandenburg, C. Dathy, P. Dorenbos, S. Kraft, R. Ostendorf, V. Ouspenski, and A. Owens, Nuclear Instruments and Methods in Physics Research Section A: Accelerators, Spectrometers, Detectors and Associated Equipment **574**, 115 (2007), ISSN 0168-9002.
- [8] G. Pausch, C.-m. Herbach, R. Hillebrands, A. Kreuels, R. Lentering, F. Lueck, F. Platte, C. Plettner, K. Roemer, F. Scherwinski, et al., in *2007 IEEE Nuclear Science Symposium Conference Record* (IEEE, 2007), vol. 3, pp. 963–968, ISBN 978-1-4244-0922-8.
- [9] R. Devanathan, L. Corrales, F. Gao, and W. Weber, Nuclear Instruments and Methods in Physics Research Section A: Accelerators, Spectrometers, Detectors and Associated Equipment **565**, 637 (2006), ISSN 0168-9002.
- [10] D. L. Smith, H. Mach, H. Penttilä, H. Bradley, J. Äystö, V.-V. Elomaa, T. Eronen, D. G. Ghiță, J. Hakala, M. Hauth, et al., Phys. Rev. C **77**, 014309 (2008).
- [11] J.-M. Régis, G. Pascovici, J. Jolie, and M. Rudigier, Nuclear Instruments and Methods in Physics Research Section A: Accelerators, Spectrometers, Detectors and Associated Equipment **622**, 83 (2010), ISSN 0168-9002.
- [12] W. W. Moses and K. S. Shah, Nuclear Instruments and Methods in Physics Research Section A: Accelerators, Spectrometers, Detectors and Associated Equipment **537**, 317 (2005), ISSN 0168-9002, proceedings of the 7th International Conference on Inorganic Scintillators and their Use in Scientific and Industrial Applications.
- [13] S. Kurosawa, H. Kubo, K. Hattori, C. Ida, S. Iwaki, S. Kabuki, A. Kubo, E. Kunieda, K. Miuchi, T. Nakahara, et al., Nuclear Instruments and Methods in Physics Research Section A: Accelerators, Spectrometers, Detectors and Associated Equipment **623**, 249 (2010), ISSN 0168-9002, 1st International Conference on Technology and Instrumentation in Particle Physics.
- [14] J. Kulisek, J. Hartwell, M. McIlwain, and R. Gardner, Nuclear Instruments and Methods in Physics Research Section A: Accelerators, Spectrometers, Detectors and Associated Equipment **580**, 226 (2007), ISSN 0168-9002, proceedings of the 10th International Symposium on Radiation Physics - ISRP 10.
- [15] B. Milbrath, B. Choate, J. Fast, W. Hensley, R. Kouzes, and J. Schweppe, Nuclear Instruments and Methods in Physics Research Section A: Accelerators, Spectrometers, Detectors and Associated Equipment **572**, 774 (2007), ISSN 0168-9002.
- [16] M. Vencelj, K. Bučar, R. Novak, and H. J. Wörtche, Nuclear Instruments and Methods in Physics Research A **607**, 581 (2009).
- [17] SIS, Struck Innovative Systeme GmbH, *Datenblatt SIS3350*, <http://www.struck.de/sis3350.htm> (2008).
- [18] B. Löher, *GECKO Data Acquisition*, <https://gitorious.org/gecko> (2012).
- [19] R. Novak and M. Vencelj, Nuclear Science, IEEE Transactions on **56**, 3680 (2009), ISSN 0018-9499.